DEUTSCHES ELEKTRONEN-SYNCHROTRON

DESY 94-009
January 1994

Inclusive Particle Production at HERA: Resolved and Direct Quasi-Real Photon Contributions in Next-to-Leading Order QCD

B. A. Kniehl, G. Kramer

II. Institut für Theoretische Physik, Universität Hamburg

ISSN 0418-9833

NOTKESTRASSE 85 - 22603 HAMBURG

To be sure that your preprints are promptly included in the
HIGH ENERGY PHYSICS INDEX,
send them to (if possible by air mail):

DESY **Bibliothek** **Notkestraße 85** **22603 Hamburg** **Germany**	**DESY-IfH** **Bibliothek** **Platanenallee 6** **15738 Zeuthen** **Germany**

DESY 94-009
January 1994

ISSN 0418-9833

Inclusive particle production at HERA: Resolved and direct quasi-real photon contributions in next-to-leading order QCD

B.A. KNIEHL AND G. KRAMER

II. Institut für Theoretische Physik,[†] *Universität Hamburg,*
Luruper Chaussee 149, D-22761 Hamburg, Germany

ABSTRACT

We calculate in next-to-leading order inclusive cross sections of single-particle production via both direct and resolved photons in ep collisions at HERA. Transverse-momentum and rapidity distributions are presented and the dependences on renormalization and factorization scales and subtraction schemes are investigated.

† *Supported by the Bundesministerium für Forschung und Technologie under Contract 05 6 HH 93P (5), Bonn, Germany*

1. Introduction

The inclusive cross section for the production of single hadrons at large transverse momentum (p_T) has always been an important testing ground for the QCD-improved parton model. For quantitative predictions it is necessary to go to the next-to-leading order (NLO) of the perturbative expansion. First partial results for hadron-hadron collisions were obtained in 1980 by Ellis et al. [1]. NLO corrections to all contributing parton-parton scattering cross sections have been completed by Aversa et al. [2] a few years ago. Using these results, we have recently studied inclusive single-particle production in $p\bar{p}$ collisions together with Borzumati in [3], henceforth referred to as I. We compared our results with UA2 and CDF experimental data and found reasonable agreement. Also the inclusive production of single hadrons at high p_T in photon-proton collisions offers the opportunity to confront perturbative QCD with experimental data, from HERA. The QCD dynamics in this process is more complicated than in hadron-hadron collisions. This is due to the fact that, at high energies, high-p_T hadrons can be produced either by direct photon-quark interactions or through the resolved photon component [4]. The latter mechanism is very similar to the hard-scattering processes triggered by hadron-hadron collisions. NLO corrections to direct photoproduction have been calculated by Aurenche et al. [5]. Their results were compared with data taken in fixed-target experiments at CERN [6]. In their analysis, resolved photoproduction was included only in leading order (LO).

Recently, together with Borzumati, we have presented in [7] (henceforth called **II**) NLO results for resolved photoproduction of charged single hadrons and compared them with first data from HERA, published by the H1 Collaboration [8]. These data were taken at rather low p_T ($p_T < 3.5$ GeV). For such low p_T, the direct-photon component is small as compared to the one due to resolved photons and could be neglected. In the meantime, measurements have been extended to higher p_T, up to about 8 GeV [9]. In **II**, we found that in LO the direct and resolved components are comparable in size at $p_T \approx 13$ GeV. To obtain reliable theoretical predictions for larger p_T, it is mandatory to evaluate both direct and resolved contributions in NLO and combine them in a consistent way. The latter point refers to the fact that the separation of the resolved and NLO direct contributions brings in a factorization scale, M_γ. The dependence on M_γ must cancel to a large extend when the two components are superimposed.

The outline of this paper is as follows. In Sect. 2, we give a brief introduction to the theoretical input and the parton density functions of the proton and photon used for the calculation. Numerical results are presented in Sect. 3, where we first concentrate on direct photoproduction, assuming the incoming photons to be *real*, and study the influence of the parton density functions and the various scale dependences. In the sequel, we consider *quasi-real* photoproduction, both in the direct and resolved modes, and present theoretical predictions in such a form that they can be compared directly with HERA data. Section 4 is reserved for a summary of the results and an outlook to future work.

2. Theoretical input and parton density functions

As is well known, there exist two distinct mechanisms which contribute to the inclusive photoproduction of hadrons at high energies. The photon can interact either directly with the partons originating from the proton, giving rise to the direct process, or via its quark and gluon content, the so-called resolved part. In both processes, partons may be produced at high p_T and fragment into single hadrons. Both contributions are of the same order in the perturbative expansion. The LO contribution of the resolved part is given by LO parton-parton scattering cross sections, multiplied by LO parton density functions of the photon and proton and LO fragmentation functions for the final hadron. Since the parton-parton scattering terms are of $\mathcal{O}\left(\alpha_s^2\right)$ and the photonic parton density functions of $\mathcal{O}(\alpha/\alpha_s)$, the LO contributions in the direct and resolved channels are both of $\mathcal{O}(\alpha\alpha_s)$. To obtain stable predictions, i.e., predictions that do not suffer so much from scale ambiguities, we must go to NLO for both resolved and direct processes. In the NLO formalism, we need the hard-scattering cross sections in NLO with two-loop $\alpha_s(\mu)$ and two-loop-evolved parton density and fragmentation functions.

To fix the notation, let us first consider photoproduction with real photons,

$$\gamma(p_\gamma) + p(p_p) \to h(p_h) + X\,, \tag{2.1}$$

where p_γ, p_p, and p_h are the momenta of the photon, proton, and outgoing hadron, respectively. The LO cross section for resolved photoproduction is given by

$$E_h \frac{d^3\sigma^0}{d^3p_h} = \sum_{i,j,l} \int dx_\gamma dx_p \frac{dx_h}{x_h^2} F_i^\gamma\left(x_\gamma, M_\gamma^2\right) F_j^p\left(x_p, M_p^2\right) \times D_l^h\left(x_h, M_h^2\right) k_l^0 \frac{d^3\sigma^0_{k_i k_j \to k_l}}{d^3k_l}\,, \tag{2.2}$$

where $k_i = x_\gamma p_\gamma$, $k_j = x_p p_p$, and $k_l = p_h/x_h$ are the parton momenta. The indices i, j, and l run over gluons and N_F flavours of quarks. We assume $N_F = 4$ throughout our calculation and include the charm-quark threshold as implemented in $F_c^\gamma(x_\gamma, Q^2)$. $F_i^\gamma\left(x_\gamma, M_\gamma^2\right)$ is the density function of parton i in the photon, $F_j^p\left(x_p, M_p^2\right)$ is the density function of parton j in the proton, and $D_l^h\left(x_h, M_h^2\right)$ is the fragmentation function of parton l into hadron h. $d^3\sigma^0_{k_i k_j \to k_l}$ is the cross section of the hard-scattering process $i + j \to l + X$ in $\mathcal{O}\left(\alpha_s^2\right)$. In the case of the direct process, $F_i^\gamma\left(x_\gamma, M_\gamma^2\right)$ is replaced by $\delta(1 - x_\gamma)$ and the hard-scattering cross section is of $\mathcal{O}(\alpha\alpha_s)$. In (2.2), we have four scales altogether: the factorization scales connected with the parton densities of the photon and proton, M_γ and M_p, respectively, the factorization scale of the fragmentation functions, M_h, and the renormalization scale, μ, of the QCD coupling constant α_s.

In LO, all four scales are left undefined, which causes considerable uncertainty for the theoretical prediction to that order. Of course, the LO direct cross section does not depend on M_γ.

In NLO, the inclusive cross section is written as

$$E_h \frac{d^3\sigma}{d^3p_h} = \sum_{i,j,l} \int dx_\gamma dx_p \frac{dx_h}{x_h^2} F_i^\gamma\left(x_\gamma, M_\gamma^2\right) F_j^p\left(x_p, M_p^2\right) \times D_l^h\left(x_h, M_h^2\right) \frac{1}{\pi s}\left[\frac{1}{v}\frac{d\sigma^0_{k_ik_j\to k_l}}{dv}(s,v;\mu^2)\delta(1-w) + \frac{\alpha_s(\mu^2)}{2\pi} K_{k_ik_j\to k_l}\left(s,v,w;\mu^2,M_\gamma^2,M_p^2,M_h^2\right)\right], \tag{2.3}$$

where $v = 1 + t/s$ and $w = -u/(s+t)$, with $s = (k_i + k_j)^2$, $t = (k_i - k_l)^2$, and $u = (k_j - k_l)^2$ being the Mandelstam variables at the parton level. The latter are related to the external Mandelstam variables, $S = (p_\gamma + p_p)^2$, $T = (p_\gamma - p_h)^2$, and $U = (p_p - p_h)^2$, by $s = x_\gamma x_p S$, $t = x_\gamma/x_h T$, and $u = x_p/x_h U$. The functions $K_{k_ik_j\to k_l}\left(s,v,w;\mu^2,M_\gamma^2,M_p^2,M_h^2\right)$ embody the NLO corrections to the hard-scattering cross sections.

In the case of resolved photoproduction, the calculation of the $K_{k_ik_j\to k_l}$ terms is described in [2], where M_γ and M_p are identified. For the purposes of the present work, we have disentangled these scales.

The NLO cross section of direct photoproduction has a structure similar to (2.3). The only difference is that $\delta(1-x_\gamma)$ is substituted for $F_i^\gamma\left(x_\gamma, M_\gamma^2\right)$. The $K_{k_ik_j\to k_l}$ terms have been calculated by Aurenche et al. [5], for $M_\gamma = M_p = M_h$. Also here we have re-evaluated the scale dependent terms so as to render possible independent variations of M_γ, M_p, and M_h. In the calculation of $K_{k_ik_j\to k_l}$, one encounters singularities associated with the incoming photon lines. These initial-state singularities are absorbed into the bare parton density functions of the resolved photon, which renders these functions M_γ dependent. In turn, a similar M_γ dependence, but with the opposite sign, shows up in the $K_{k_ik_j\to k_l}$ terms of the direct process. In this way, resolved and direct photoproduction become intermixed. The resolved part is actually a NLO contribution to the direct part that cannot, however, be treated fully perturbatively any more. This non-perturbative part is then described by the F_i^γ functions. The M_γ dependence cancels, up to higher-order terms in F_i^γ, in the combination of direct and resolved contributions. It is therefore apparent that the distinction of direct and resolved photoproduction becomes ambiguous when NLO corrections are taken into account. Terms that have been included in the NLO corrections to direct photoproduction may be shifted to the resolved part and vice versa. We shall return to this point in Sect. 3.

The calculation of the inclusive cross section of resolved photoproduction of hadrons is described in detail in **II**. For consistency, one needs the parton density functions of the photon and proton and the fragmentation functions in NLO. Fragmentation functions exist so far only in LO, except for a recently constructed π^0 set [10]. New NLO sets are being constructed, also for charged particles [11]. To facilitate comparisons with our earlier work in **I** and **II**, we shall use the same fragmentation functions as in **I**, namely those by Baier et al. [12] and Anselmino et al. [13] with the constraints specified in **I**. Since these fragmentation functions correspond approximately to the $\overline{\rm MS}$ factorization, we have, in general, also selected the $\overline{\rm MS}$ scheme of factorization in connection with the incoming legs. In the $\overline{\rm MS}$ scheme, we define the spin average for incoming gluons and photons as $1/(n-2)$, where n is the dimensionality of space-time.

The parametrizations for the parton density functions of the photon and proton are taken from the package by Charchuła [14]. As for the proton sets, we use MRS D0′ [15] for the most part of our analysis. This set is not in full agreement with recent structure-function measurements at very small x ($x \lesssim 10^{-3}$) [9]. Such low x values are relevant for single-hadron production only at very small $p_{\rm T}$, where perturbative QCD is probably not valid any more. Very recently, also the CTEQ Collaboration has published several proton sets [16], which we use for comparisons in some cases. They reach down to lower Q^2 values than the latest MRS sets.

For NLO photonic parton density functions, we use the sets by Glück, Reya, and Vogt (GRV) [17]. In their analysis, the Q^2 evolution starts at a rather low value, $Q_0^2 = 0.3$ GeV^2. Therefore, this set is applicable also at rather small $p_{\rm T}$; however, one should keep in mind that the predictions may not be very reliable in this regime because α_s is large. Other NLO sets have been introduced by Aurenche et al. [18] and Gordon and Storrow [19]. The latter authors use $Q_0^2 = 5.3$ GeV^2, which is less useful for our purposes.

In Sect. 3, we present the results in two steps. In the first step, we investigate the NLO corrections to direct photoproduction in some detail, taking the incoming photon to be real. We recall that resolved photoproduction has been studied in great detail already in **II**. In the second step, we superimpose the direct and resolved contributions to photoproduction in ep collisions so as to obtain reliable predictions, which are suitable for direct comparisons with HERA data, especially at larger $p_{\rm T}$. Here, we also study how the M_γ dependences of direct and resolved contributions compensate each other.

3. Numerical results

3.1. NLO corrections to direct photoproduction

In this subsection, we present inclusive cross sections for photoproduction of charged hadrons via direct photons, which are taken to be real. We employ the MRS D0′ parton density functions of the proton in the $\overline{\rm MS}$ scheme and the same fragmentation functions as in **I** and **II** and include four quark flavours. To conform with HERA conventions, we sum over charged hadrons, $h^+ + h^-$, where $h^\pm$ are charged pions and kaons. This is in contrast to **I** and **II**, where we considered the average,

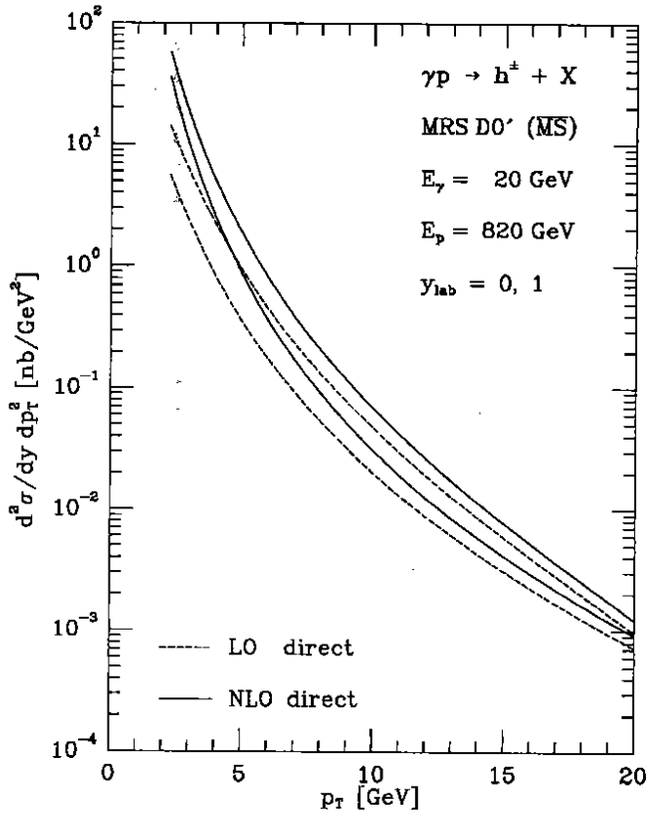

Fig. 1. p_T distributions of $\gamma p \to h^{\pm} + X$ via direct photons to NLO in the $\overline{\rm MS}$ scheme at $\sqrt{s} = 256$ GeV and $y_{\rm lab} = 0, 1$ (solid lines). The MRS D0′ set is used and $\mu = M_\gamma = M_p = M_h = p_T$ is chosen. For comparison, also the evaluations with $K_{k_i k_j \to k_l} = 0$ are shown (dashed lines). The upper lines refer to $y_{\rm lab} = 0$

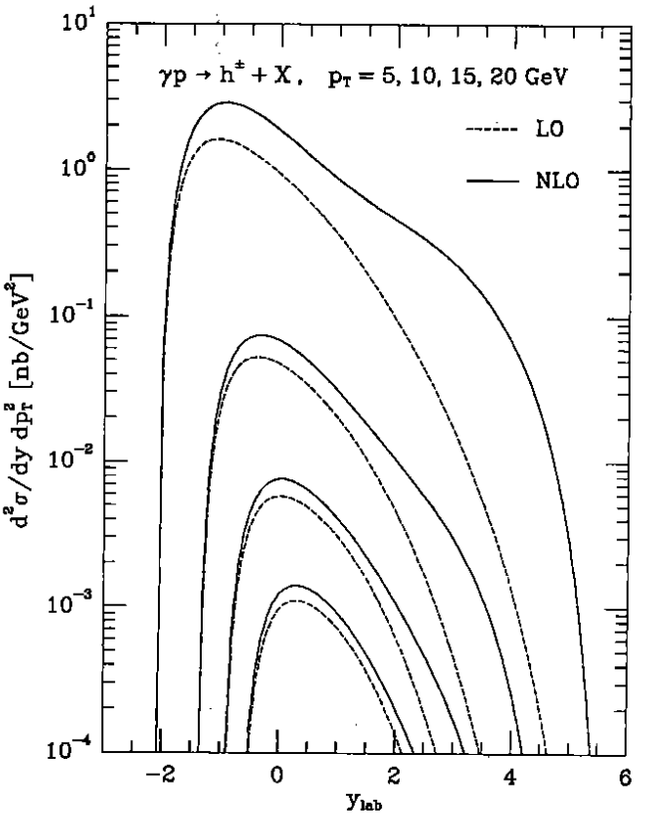

Fig. 2. $y_{\rm lab}$ distributions of $\gamma p \to h^{\pm} + X$ via direct photons to NLO in the $\overline{\rm MS}$ scheme at $\sqrt{s} = 256$ GeV and $p_T = 5, 10, 15, 20$ GeV (solid lines). The MRS D0′ set is used and $\mu = M_\gamma = M_p = M_h = p_T$ is chosen. For comparison, also the evaluations with $K_{k_i k_j \to k_l} = 0$ are shown (dashed lines). Lower-lying lines correspond to larger p_T

$(h^+ + h^-)/2$. (Charged-baryon production is negligibly small.) For the same reason, we also alter the orientation of the rapidity axis; $y_{\rm lab} > 0$ now corresponds to the direction of the incident proton. To select typical HERA conditions, we consider collisions of 820 GeV protons on 20 GeV photons, which corresponds to a centre-of-mass energy of $\sqrt{s} = 256$ GeV. We evaluate α_s at two loops, and set the asymptotic scale parameter, Λ, in α_s equal to the value required by the parton density functions of the proton, i.e., 230 MeV in the case of the MRS D0′ set. Our standard choice of scales is $\mu = M_\gamma = M_p = M_h = p_T$, except when we investigate the various scale dependences.

We first study the size of the NLO corrections to the parton-level cross section. In Fig. 1, the cross section, $d^2\sigma/dy\,dp_T^2$, is shown as a function of p_T for $y_{\rm lab} = 0, 1$. The upper curves correspond to $y_{\rm lab} = 0$. The solid lines represent the NLO calculation described above; the dashed lines are obtained by setting the $K_{k_i k_j \to k_l}$ functions to zero, but keeping α_s and the parton density functions at NLO. We see that, in the $y_{\rm lab}$ and p_T range considered, the NLO corrections are positive and quite substantial. The K factor, i.e., the ratio of the two evaluations, ranges between 1.3 and 6.3, being larger at smaller p_T. Furthermore, we see that it varies with $y_{\rm lab}$, too; it is larger at positive $y_{\rm lab}$. To investigate this feature more in detail, we plot, in Fig. 2, $d^2\sigma/dy\,dp_T^2$ versus $y_{\rm lab}$ for $p_T = 5$, 10, 15, and 20 GeV. It is striking that the K factor becomes very large towards the kinematic boundary at $y_{\rm lab} > 0$, especially for small p_T. This effect diminishes with increasing p_T. Detailed analysis reveals that this feature is mainly attributed to a channel which is absent in LO, namely $\gamma g \to g + X$. Obviously, the LO prediction of direct photoproduction fails badly at small p_T and large positive $y_{\rm lab}$. However, as we shall see later, direct photoproduction makes up only a small fraction of the full result in this kinematic regime anyway.

So far, we have used the common scale $\mu = M_\gamma = M_p = M_h = p_T$. In Figs. 3a–c, we investigate the scale dependences of $d^2\sigma/dy\,dp_T^2$ for $y_{\rm lab} = 0$ and $p_T = 5$, 15, and 25 GeV, respectively. To that end, we introduce a dimensionless scale parameter, ξ. In each figure, the evaluation is performed

1) in LO with $\mu = M_p = M_h = \xi p_T$ (dashed line),
2) in NLO with $M_\gamma = \xi p_T$ and $\mu = M_p = M_h = p_T$ (dash-dotted line), and
3) in NLO with $\mu = M_p = M_h = \xi p_T$ and $M_\gamma = p_T$ (solid line).

Here LO bears the same meaning as in Figs. 1 and 2. In case 2), where we vary only the factorization scale attached to the photon leg, M_γ, we obtain a straight line, i.e., we recover the characteristic scale dependence

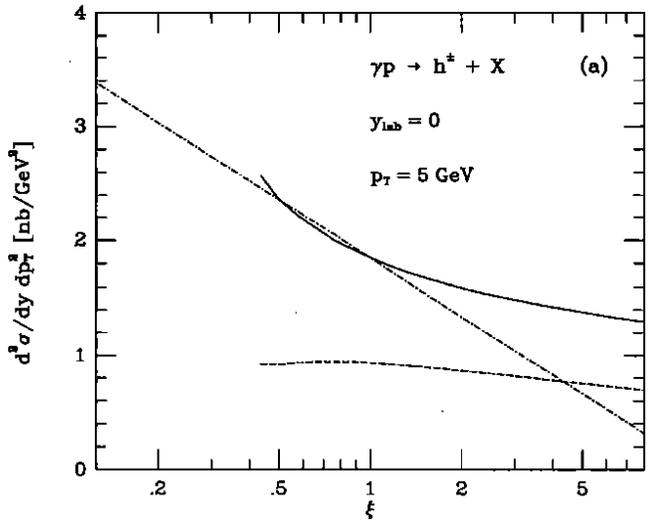

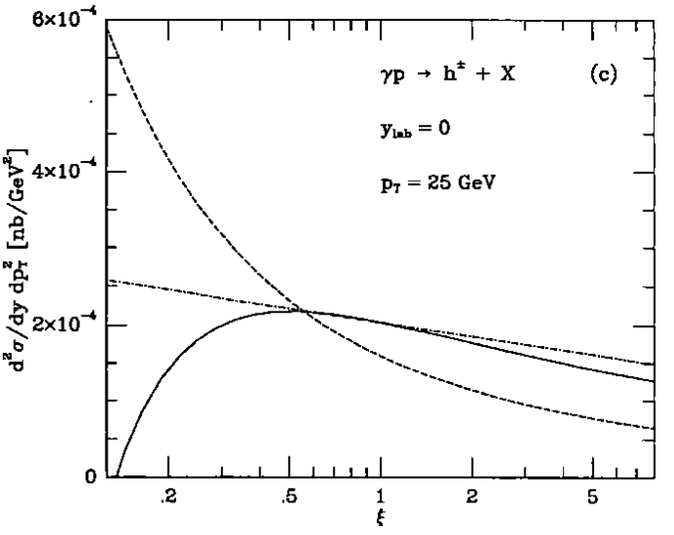

Fig. 3a,b,c. Scale dependences of $d^2\sigma/dy\,dp_T^2$ for $\gamma p \to h^\pm + X$ via direct photons to NLO in the $\overline{\rm MS}$ scheme at $\sqrt{s} = 256$ GeV, $y_{\rm lab} = 0$, and $p_T = 5, 15, 25$ GeV, respectively. The dot-dashed (solid) lines are evaluated with $M_\gamma = \xi p_T$ and $\mu = M_p = M_h = p_T$ ($\mu = M_p = M_h = \xi p_T$ and $M_\gamma = p_T$). The MRS D0′ set is used. The dashed lines emerge from the solid lines by setting $K_{k_i k_j \to k_l} = 0$

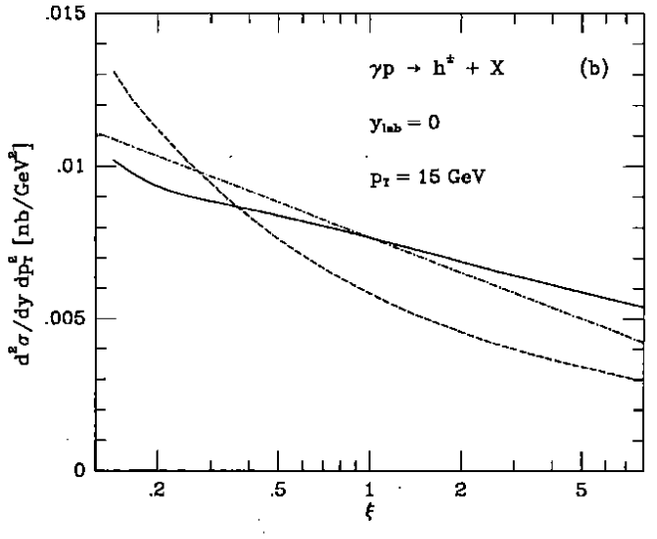

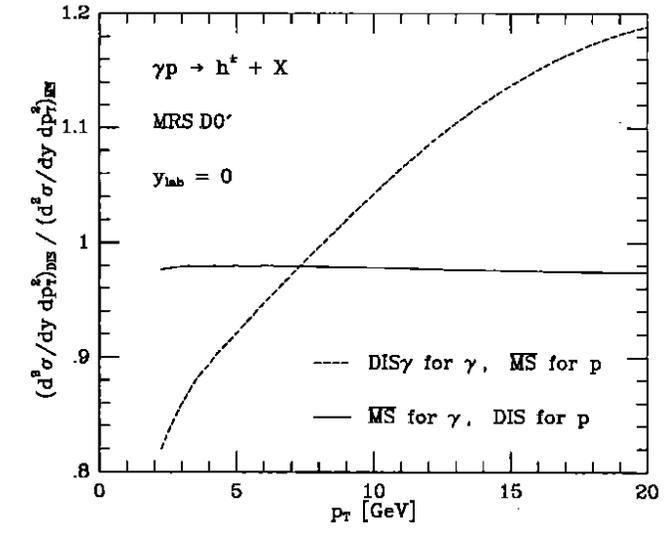

Fig. 4. p_T distributions of $\gamma p \to h^\pm + X$ via direct photons to NLO at $\sqrt{s} = 256$ GeV and $y_{\rm lab} = 0$ evaluated using in turn the DISγ scheme for the photon and the $\overline{\rm MS}$ scheme for the proton (dashed line) and the $\overline{\rm MS}$ scheme for the photon and the DIS scheme for the proton (solid line). The results are normalized to the corresponding calculation where the $\overline{\rm MS}$ scheme is used throughout (cf. Fig. 1). The MRS D0′ set is used and $\mu = M_\gamma = M_p = M_h = p_T$ is chosen

$a + b \ln \xi$. As mentioned above, there is no M_γ dependence at LO. When all scales, except for M_γ, are varied simultaneously, the ξ dependence is, in general, increased as we switch off the $K_{k_i k_j \to k_l}$ terms, i.e., as we pass from case 3) to case 1). However, this is true only if p_T is large enough. At $p_T = 5$ GeV, the LO result is almost independent of ξ. In this case, a large compensation between the individual variations with μ, M_p, and M_h is at work. In Figs. 3a and b, the results corresponding to cases 1) and 3) are shown only for $\xi \geq Q_0/p_T$, where $Q_0 = \sqrt{5}$ GeV is the starting point of the Q^2 evolution implemented in the MRS D0′ set. For lower values of ξ, no meaningful results are obtained. In particular, we observe that, at $p_T = 15$ GeV, the cross section changes by no more than 20% in NLO as compared to 70% in LO when the scales are varied between $p_T/2$ and $2p_T$. Similar studies of the scale dependence have been reported for resolved photoproduction in **II**.

A further source of uncertainty is the choice of subtraction scheme for the parton density and fragmentation functions. This point can be studied only in NLO, where the respective finite changes in these functions are supposed to be compensated by equivalent shifts in the $K_{k_i k_j \to k_l}$ terms. To test this compensation, we compute $d^2\sigma/dy\,dp_T^2$ at $y_{\rm lab} = 0$ as a function of p_T using the deep-inelastic scattering (DIS) scheme of subtraction at the proton leg, along with the appropriate MRS D0′ set, and plot the ratio of this evaluation to the one using the $\overline{\rm MS}$ scheme (cf. Fig. 1) in Fig. 4 (solid line). Specifically,

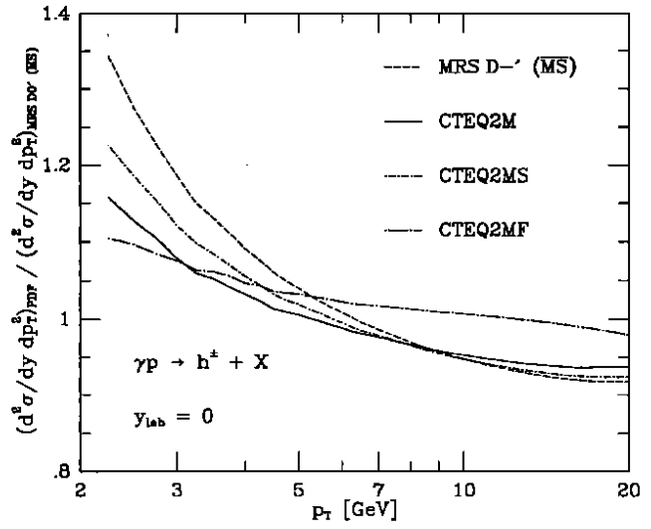

Fig. 5. p_T distributions of $\gamma p \to h^{\pm} + X$ via direct photons to NLO in the $\overline{\text{MS}}$ scheme at $\sqrt{s} = 256$ GeV and $y_{\text{lab}} = 0$ evaluated using in turn the MRS D−′ (dashed line), CTEQ2M (solid line), CTEQ2MS (dot-dashed line), and CTEQ2MF (dot-long-dashed line) sets. The results are normalized to the corresponding calculation with the MRS D0′ set. $\mu = M_\gamma = M_p = M_h = p_T$ is chosen

we modify the $K_{k_i k_j \to k_l}$ functions according to the DIS conventions by Diemoz et al. [20], i.e., the spin average for an incoming gluon is taken to be $1/2$ and the finite shifts are defined as

$$f_{qq}(x) = C_F \left[(1+x^2) \left(\frac{\ln(1-x)}{1-x} \right)_+ - \frac{3}{2} \left(\frac{1}{1-x} \right)_+ - \frac{1+x^2}{1-x} \ln x + 3 + 2x - \left(\frac{9}{2} + \frac{\pi^2}{3} \right) \delta(1-x) \right],$$

$$f_{gq}(x) = -f_{qq}(x),$$

$$f_{qg}(x) = \frac{1}{2} \left\{ \left[x^2 + (1-x)^2 \right] \ln \frac{1-x}{x} + 6x(1-x) \right\},$$

$$f_{gg}(x) = -2N_F f_{qg}(x). \qquad (3.1)$$

We recall that, in the $\overline{\text{MS}}$ scheme, these functions are all set to zero and the spin average for an initial-state gluon is chosen to be $1/(n-2)$, where n is the dimensionality of space-time. We see that the transition from the $\overline{\text{MS}}$ to the DIS scheme of subtraction at the proton leg leads to a negligible decrease, by approximately 2%, for all p_T values considered. In the resolved cross section, the subtraction scheme for the photonic parton density functions can be changed in a similar way. Glück, Reya, and Vogt [17] implemented the so-called DISγ scheme in their parametrizations. In this case, terms that are singular near $x = 1$ are shifted from the resolved cross section to the direct one. This necessarily produces a different direct cross section. The ratio of the direct cross section in the DISγ scheme to the $\overline{\text{MS}}$ result (cf. Fig. 1) is also shown in Fig. 4 (dashed line). This ratio increases by almost 50% as p_T runs from 2 to 20 GeV.

Unfortunately, also the parton density functions of the proton are not unique. Different authors favour different experimental input or make different assumptions concerning the functional x dependence of the input distributions at scale Q_0. To study such variations, we calculate $d^2\sigma/dy\,dp_T^2$ at $y_{\text{lab}} = 0$ as a function of p_T to NLO in the $\overline{\text{MS}}$ scheme using in turn various recent sets by the MRS and CTEQ collaborations, namely MRS D−′ [15], CTEQ2M, CTEQ2MS, and CTEQ2MF [16]. In Fig. 5, we show the ratios of the resulting cross sections to the previous calculation, with the MRS D0′ [15] set. The wiggles in some of the curves reflect the numerical error of our computation. These sets differ mainly in the small-x behaviour of the gluon and sea-quark densities, which are only feebly constrained by present data. This behaviour is assumed to be flat (steep) in the MRS D0′ and CTEQ2MF (MRS D−′ and CTEQ2MS) sets; CTEQ2M corresponds to the best fit of [16]. The ratios do not differ very much from 1. For $p_T \gtrsim 4$ GeV, the relative deviations do not exceed 10%. Only at rather small p_T ($p_T \lesssim 3$ GeV), where perturbative QCD may not be very predictive anyway, the discrepancies become significant. We see that the MRS D−′ and CTEQ2MS sets give similar results, which are most enhanced in the small-p_T range. This is due to the singular small-x behaviour of the gluon and sea-quark distributions, which should become visible at small p_T. The evaluations with MRS D0′ and CTEQ2MF differ by less than 10% from each other over the whole p_T range considered.

3.2. Single-charged-hadron production in ep collisions

In this subsection, we present inclusive cross sections for photoproduction of single charged hadrons in ep collisions, both via direct and resolved quasi-real photons. According to present HERA conditions, we take the energies of electrons and protons in the laboratory frame to be 26.7 and 820 GeV, respectively, so that $\sqrt{s} = 296$ GeV. We calculate the energy spectrum of the resulting photons with the following formula [19]:

$$f_{\gamma/e}(x) = \frac{\alpha}{2\pi} \left[\frac{1+(1-x)^2}{x} \ln \frac{Q^2_{\text{max}}}{Q^2_{\text{min}}} - \frac{2(1-x)}{x} \right], \qquad (3.2)$$

where $x = p_\gamma / E_e$ is the longitudinal-momentum fraction, $Q^2_{\text{max}} = 0.01$ GeV^2 is chosen as in the H1 experimental set-up with photon tagging, and $Q^2_{\text{min}} = m_e^2 x^2/(1-x)$, with m_e being the electron mass. The above formula is an extension of the traditionally applied Weizsäcker-Williams approximation (WWA). In the WWA, the term $-(\alpha/\pi)(1-x)/x$ does not appear. In the present situation, it is a non-negligible correction, in particular for tagged photons, where Q^2_{max} is so small. In conformity with the cuts applied in the H1 experiment, we exclude x values outside the interval $0.3 < x < 0.7$. Equation (3.2) together with this x cut determines the photon luminosity employed in our calculation.[1]

[1] In II, we used a different formula for $f_{\gamma/e}(x)$ with an angular cut of 5° and without the second term of Eq. (3.2).

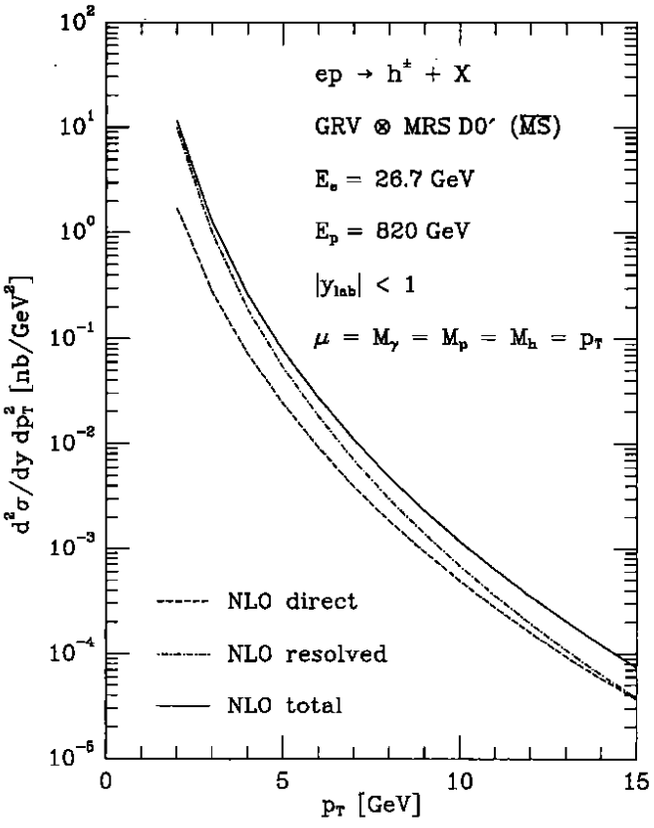

Fig. 6. p_T distributions of $ep \to h^{\pm} + X$ via direct (dashed line) and resolved (dot-dashed line) photons and their superposition (solid line) to NLO in the $\overline{\rm MS}$ scheme at $\sqrt{s} = 296$ GeV and averaged over $|y_{\rm lab}| < 1$. The GRV and MRS D0′ sets are used and $\mu = M_\gamma = M_p = M_h = p_T$ is chosen

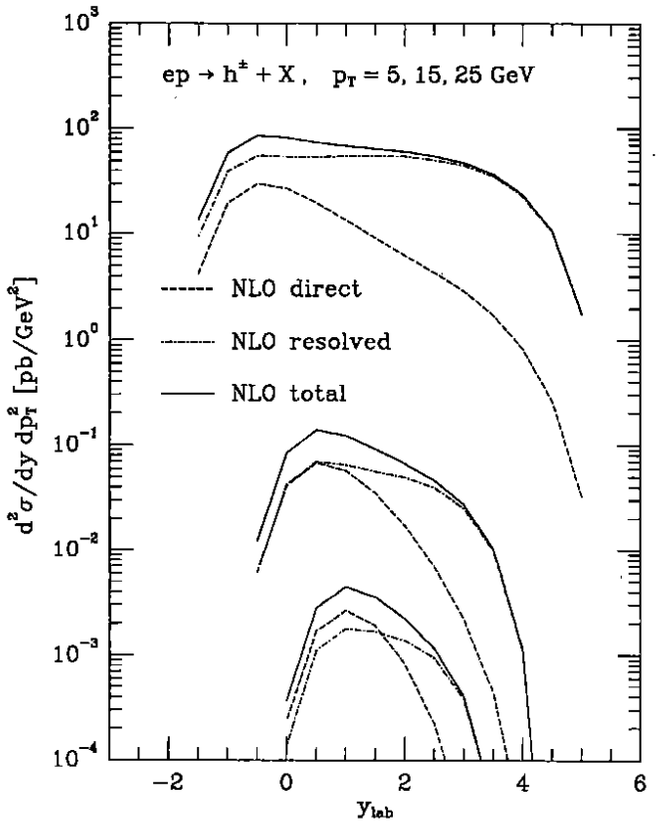

Fig. 7. $y_{\rm lab}$ distributions of $ep \to h^{\pm} + X$ via direct (dashed line) and resolved (dot-dashed line) photons and their superposition (solid line) to NLO in the $\overline{\rm MS}$ scheme at $\sqrt{s} = 296$ GeV and $p_T = 5, 15, 25$ GeV. The GRV and MRS D0′ sets are used and $\mu = M_\gamma = M_p = M_h = p_T$ is chosen

The inclusive cross section of single-particle production in ep collisions as measured with the H1 detector at HERA is related to the corresponding real-photoproduction cross section, discussed in Sect. 2, by

$$E_h \frac{d^3\sigma(ep \to h + X)}{d^3p_h} = \int_{x_{\rm min}}^{x_{\rm max}} dx\, f_{\gamma/e}(x) \times E_h \frac{d^3\sigma(\gamma p \to h + X)}{d^3p_h} . \quad (3.3)$$

On the right-hand side, $p_\gamma = xE_e$ must be substituted and $x_{\rm min}$ and $x_{\rm max}$ are determined by the experimental cuts.

As explained in the Introduction, an interesting question is how the inclusive cross section of single-particle production behaves at large p_T when the resolved and direct components are summed. The answer is given in Fig. 6, where the NLO cross sections for direct and resolved photoproduction and their sum are plotted as a function of p_T. According to the H1 acceptance cuts, the cross section is averaged over the rapidity interval $|y_{\rm lab}| < 1$. We select the GRV and MRS D0′ NLO sets, both in the $\overline{\rm MS}$ scheme. Our choice of scales is $\mu = M_\gamma = M_p = M_h = p_T$. In the evaluation of the NLO resolved component, we choose to multiply both the LO hard-scattering cross sections and the NLO corrections by the NLO photonic parton density functions, i.e., we do not adopt the prescription of [17], where it is proposed to use the LO set in connection with the NLO corrections. The difference between these two procedures is beyond NLO and may be considered as a theoretical uncertainty. A quantitative discussion of this point may be found in **II**. We see that the resolved part clearly dominates at small p_T, but falls off with increasing p_T more rapidly than the direct part; the two parts intersect at $p_T \approx 15$ GeV. As a consequence, the total cross section, i.e., the sum of the direct and resolved parts, tails off with increasing p_T more slowly than the resolved cross section alone, which we computed in **II**.

The effect of the direct component is most visible in the electron-beam direction, i.e., towards the negative end of the $y_{\rm lab}$ spectrum, provided that p_T is sufficiently large. To visualize this, we plot in Fig. 7 the direct and resolved components of $d^2\sigma/dy\,dp_T^2$ at NLO and their superposition as a function of $y_{\rm lab}$ for $p_T = 5$, 15, and 25 GeV. The evaluated points are connected by straight lines. At $p_T = 15$ GeV, the direct and resolved contributions are approximately equal for $y_{\rm lab} \lesssim 1$ (cf. Fig. 6, where we averaged over $|y_{\rm lab}| < 1$).

In **II**, we found moderate NLO corrections to the resolved γp and ep cross sections, except at low p_T. In Sect. 3.1, we made similar observations for the direct γp cross section (cf. Figs. 1 and 2). In Fig. 8, we present the

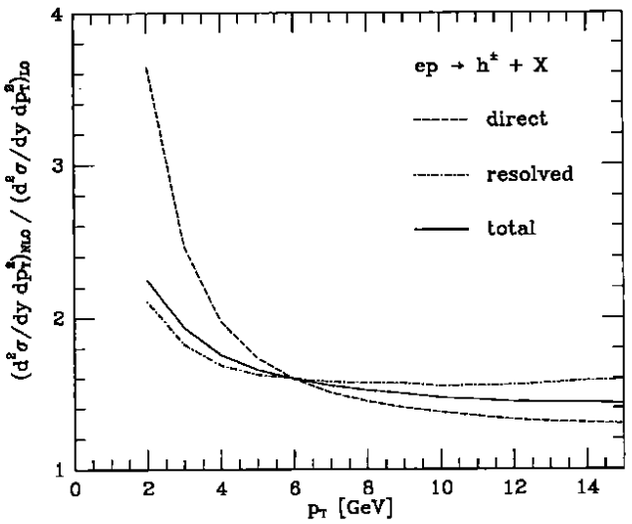

Fig. 8. Results of Fig. 6 normalized to the respective evaluations with $K_{k_i k_j \to k_l} = 0$

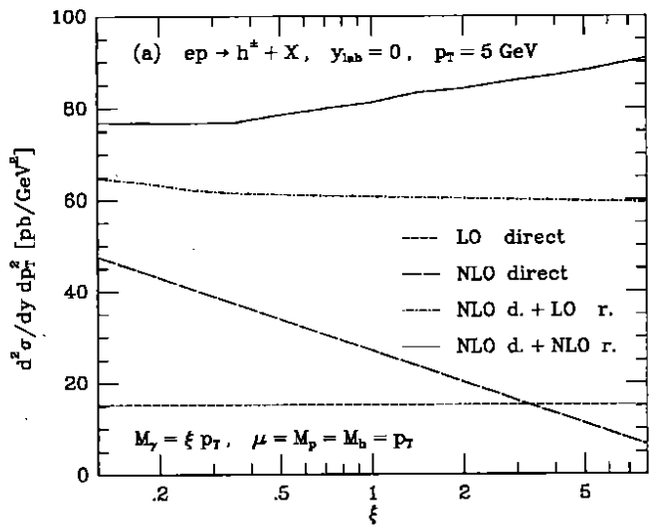

Fig. 9a,b,c. M_γ dependences ($M_\gamma = \xi p_T$) of $d^2\sigma/dy\,dp_T^2$ for $ep \to h^\pm + X$ via photoproduction in the $\overline{\rm MS}$ scheme at $\sqrt{s} = 296$ GeV, $y_{\rm lab} = 0$, and $p_T = 5, 15, 25$ GeV, respectively. The GRV and MRS D0′ sets are used and $\mu = M_p = M_h = p_T$ is chosen. Starting from the LO direct cross section (dashed line), we add in turn the NLO corrections to the direct cross section (long-dashed line), the LO resolved cross section (dot-dashed line), and the NLO corrections to the resolved cross section (solid line)

ratios of the direct, resolved, and total ep cross sections at NLO shown in Fig. 6 to the respective evaluations with the $K_{k_i k_j \to k_l}$ terms omitted. We see that, in the region where the QCD-improved parton model is expected to yield reliable predictions, $p_T \gtrsim 5$ GeV, the increase due to the NLO corrections is relatively moderate, below 65%.

We emphasized already in Sect. 3.1 that the splitting of the inclusive cross section into a direct and a resolved part is ambiguous. The ep results presented so far have been obtained for a fixed scale $M_\gamma = p_T$ and

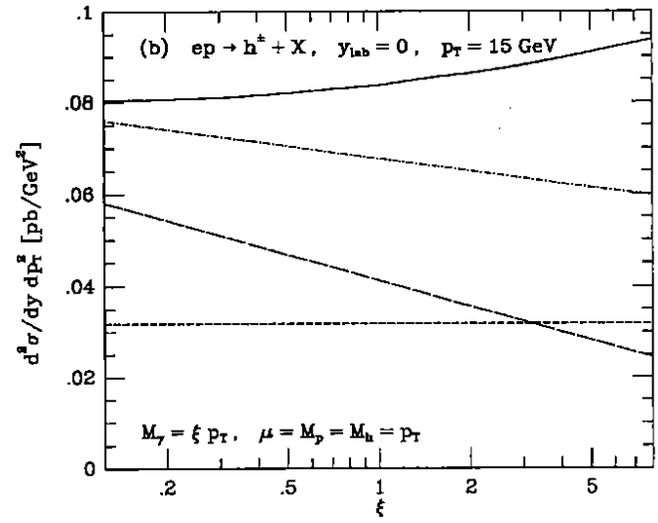

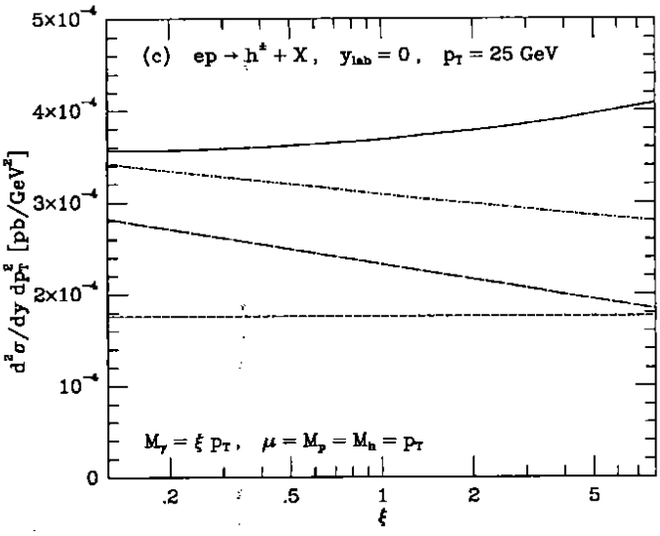

a definite subtraction scheme for the photonic parton density functions, namely the $\overline{\rm MS}$ scheme. The relation of the direct and resolved components varies with the choice of M_γ and/or factorization scheme. For example, if we put $M_\gamma = \xi p_T$ and vary ξ, then the NLO direct part changes logarithmically with $\ln\xi$ (cf. Figs. 3a–c dealing with γp scattering). This must be compensated already by the LO resolved cross section. This compensation is demonstrated in Figs. 9a–c, where we show $d^2\sigma/dy\,dp_T^2$ for $ep \to h^\pm + X$ at $y_{\rm lab} = 0$ and $p_T = 5$, 15, and 25 GeV, respectively, as a function of ξ, keeping all other scales fixed at p_T. Of course, the LO direct cross section is independent of ξ (dashed lines). The NLO direct cross section is a decreasing monomial in $\ln\xi$ (long-dashed lines). As expected, the ξ dependence is significantly reduced when the NLO direct and LO resolved contributions are combined (dot-dashed lines); this compensation works almost perfectly at $p_T = 5$ GeV (see Fig. 9a). A complete cancellation is beyond the scope of finite-order perturbation theory; there are always uncompensated terms in the next order beyond current knowledge. We also show the sum of the NLO direct and NLO resolved cross sections, which now feebly

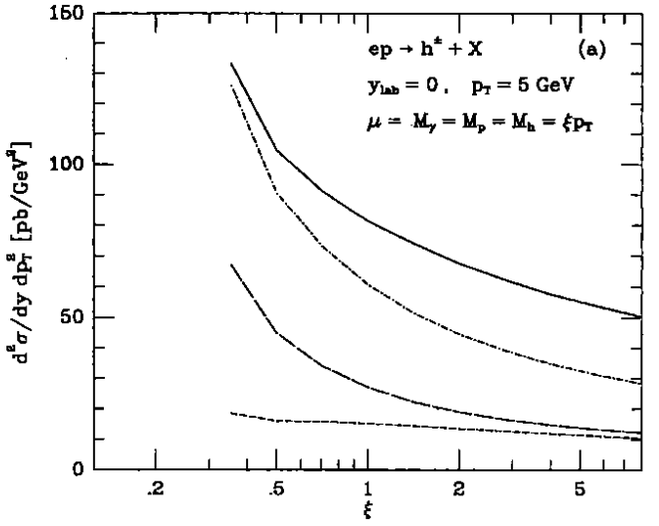

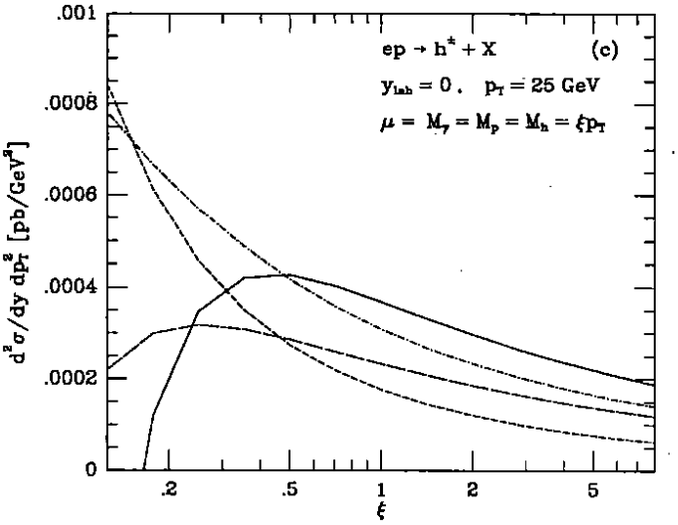

Fig. 10a,b,c. Global scale dependences ($\mu = M_\gamma = M_p = M_h = \xi p_T$) of $d^2\sigma/dy\,dp_T^2$ for $ep \to h^\pm + X$ via photoproduction in the $\overline{\rm MS}$ scheme at $\sqrt{s} = 296$ GeV, $y_{\rm lab} = 0$, and $p_T = 5, 15, 25$ GeV, respectively. The GRV and MRS D0′ sets are used. Starting from the LO direct cross section (dashed line), we add in turn the NLO corrections to the direct cross section (long-dashed line), the LO resolved cross section (dot-dashed line), and the NLO corrections to the resolved cross section (solid line)

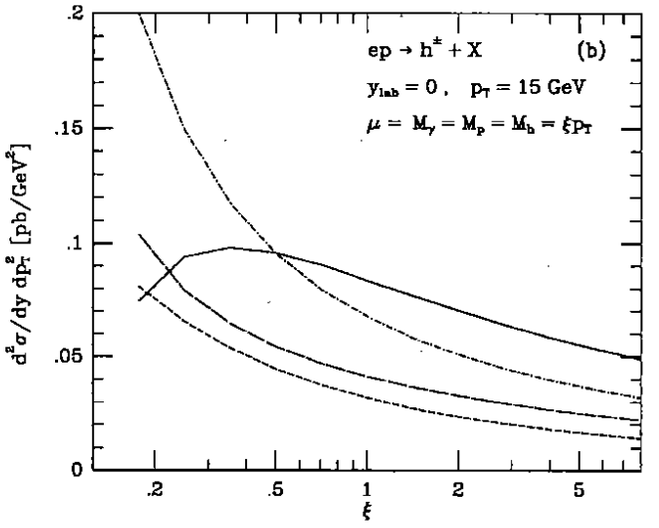

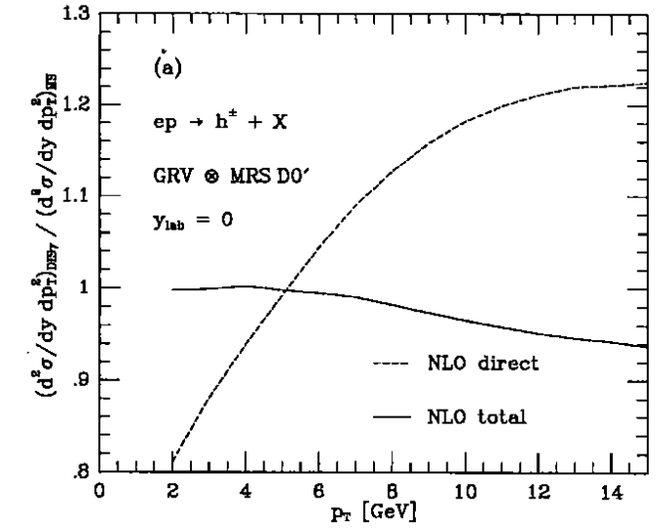

Fig. 11a,b. p_T distributions of $ep \to h^\pm + X$ via direct photons (dashed line) and direct plus resolved photons (solid line) to NLO at $\sqrt{s} = 296$ GeV and $y_{\rm lab} = 0, 1$, respectively, evaluated using the DISγ scheme for the photon and the $\overline{\rm MS}$ scheme for the proton. The results are normalized to the corresponding calculations where the $\overline{\rm MS}$ scheme is used throughout. The GRV and MRS D0′ sets are used and $\mu = M_\gamma = M_p = M_h = p_T$ is chosen

increases with ξ, but stays tolerably constant over the central range $0.5 < \xi < 2$, which is usually considered in connection with scale variations.

The global scale dependence, i.e., the one generated by setting $\mu = M_\gamma = M_p = M_h = \xi p_T$ and varying ξ, is investigated in Figs. 10a–c for $y_{\rm lab} = 0$ and $p_T = 5$, 15, and 25 GeV, respectively. It is much stronger than the M_γ dependence alone, in particular at $p_T = 5$ GeV (see Fig. 10a). At this p_T value, the LO cross section is incidentally the most stable one, which is due to large cancellations among the various scale dependences. At higher p_T, the summed NLO cross section (NLO direct plus NLO resolved) is much more stable than the LO direct one. The $p_T = 25$ GeV case is a typical example where the global scale dependence is appreciably reduced when NLO corrections are included. In fact, here we observe two successive compensations, one in the direct channel as we pass from the dashed line to the long-dashed one and another one in the resolved channel as we pass from the dot-dashed line to the solid one. From Figs. 10a–c we read off a theoretical uncertainty of 30% and 20% for $p_T = 5$ GeV and $p_T \geq 15$ GeV, respectively, due to a global scale variation in the range $0.5 < \xi < 2$.

In Sect. 3.2, we studied the variation of the direct γp cross section at NLO under a change of the factorization scheme for the photonic parton density functions, from the $\overline{\rm MS}$ to the DISγ scheme. Except for p_T values in the vicinity of some fixed point, we found a dramatic shift (cf. Fig. 4). In Figs. 11a and b, we perform a

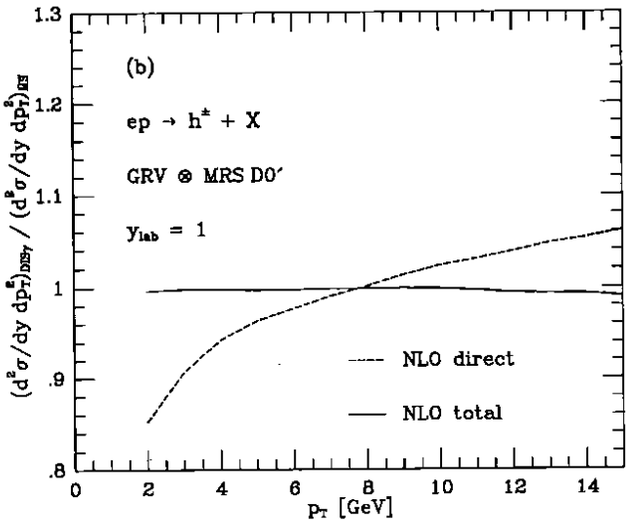

similar study for the NLO ep cross section at $y_{\rm lab} = 0$ and 1, respectively. The NLO direct component (dashed lines) exhibits the same qualitative features as before, while the sum of the NLO direct and NLO resolved components (solid lines) is considerably less affected by the change from the $\overline{\rm MS}$ to the DISγ scheme. In the latter case, the relative deviation amounts to less than 6% in the $p_{\rm T}$ range considered. This nicely demonstrates that the NLO prediction of the total cross section is not jeopardized by theoretical uncertainties related to the choice of factorization scheme used at the photon leg. Of course, both direct and resolved components depend separately on that scheme, which gives support to the notion that only their sum is meaningful physically.

4. Summary and outlook

We have calculated in next-to-leading order (NLO) inclusive cross sections for direct and resolved photoproduction of single charged hadrons at HERA. The main new feature of the present analysis is the inclusion of the direct-photon contribution at NLO, which we neglected altogether in our previous report [7]. This is particularly important for $p_{\rm T} \gtrsim 15$ GeV, where more single charged hadrons are produced via direct photons than via resolved ones.

The NLO corrections to direct photoproduction are generally positive. They are largest for positive $y_{\rm lab}$ and small $p_{\rm T}$, i.e., in the regime where single-charged-hadron production at HERA proceeds dominantly through the resolved-photon mechanism. Even under such circumstances, however, the NLO direct contribution almost perfectly compensates the dependence of the resolved contribution on the factorization scale, M_γ, in the photonic parton density functions. The dependences on the renormalization scale, μ, and the residual factorization scales, M_p and M_h, are largely reduced within the resolved and direct channels separately when the respective NLO corrections are included, especially in the upper $p_{\rm T}$ range. This indicates that our results lend themselves to absolute predictions, in particular at large $p_{\rm T}$. On the other hand, we cannot warrant reliability of our NLO analysis in the very-low-$p_{\rm T}$ range, since there the QCD expansion parameter is too large.

Another restriction of our analysis is related to the use of LO fragmentation functions. We expect the M_h dependence to be further reduced when two-loop evolved fragmentation functions are utilized. This point is currently under study.

Acknowledgement. We thank James Botts for information on the low-Q^2 behaviour of the parton density functions of [16], Christian Gapp for providing us with a Fortran implementation of the results of [5], and Michel Fontannaz for several very helpful communications regarding [5].

References

1. R.K. Ellis, M.A. Furman, H.E. Haber, I. Hinchliffe: Nucl. Phys. B173 (1980)397
2. F. Aversa, P. Chiappetta, M. Greco, J.Ph. Guillet: Phys. Lett. B210 (1988) 225; ibid. B211 (1988) 465; Nucl. Phys. B327 (1989) 105
3. F.M. Borzumati, B.A. Kniehl, G. Kramer: Z. Phys. C57 (1993) 595
4. S.J. Brodsky, T.A. DeGrand, J.F. Gunion, J.H. Weis: Phys. Rev. Lett. 41 (1978) 672; Phys. Rev. D19 (1979) 1418; C.H. Llewellyn Smith: Phys. Lett. 79B (1978) 83; M. Drees, R.M. Godbole: Phys. Rev. Lett. 61 (1988) 682
5. P. Aurenche, R. Baier, A. Douiri, M. Fontannaz, D. Schiff: Nucl. Phys. B286 (1987) 553
6. R.J. Apsimon et al., OMEGA Photon Coll.: Z. Phys. C43 (1989) 63
7. F.M. Borzumati, B.A. Kniehl, G. Kramer: Z. Phys. C59 (1993) 341
8. T. Ahmed et al., H1 Coll.: Phys. Lett. B297 (1992) 205
9. A. De Roeck: DESY Report No. 94-005 (January 1994); also in: Proceedings of the International Europhysics Conference on High Energy Physics, Marseille, France, 1993, J. Carr and M. Perrottet (eds.), Gif-sur-Yvette: Editions Frontières 1994 (to appear); J. Dainton: RAL Report 1993; also in: Proceedings of the XVI International Symposium on Lepton-Photon Interactions, Cornell University, Ithaca, New York, 1993 (to appear)
10. P. Chiappetta, M. Greco, J.-Ph. Guillet, S. Rolli, M. Werlen: Preprint CPT-92/PE.2841, ENSLAPP-A-416/93, FNT/T-92/46, IPNL 93-1 (December 1992)
11. B. Webber: private communication
12. R. Baier, J. Engels, B. Petersson: Z. Phys. C2 (1979) 265
13. M. Anselmino, P. Kroll, E. Leader: Z. Phys. C18 (1983) 307
14. K. Charchuła: Comput. Phys. Commun. 69 (1992) 360
15. A.D. Martin, W.J. Stirling, R.G. Roberts: Phys. Lett. B306 (1993) 145; (E) B309 (1993) 492
16. J.F. Botts, H.L. Lai, J.G. Morfin, J.F. Owens. J. Qiu, W.-K. Tung: Michigan State University Report No. MSUHEP-93/28
17. M. Glück, E. Reya, A. Vogt: Phys. Rev. D45 (1992) 3986; ibid. D46 (1992) 1973
18. P. Aurenche, P. Chiappetta, M. Fontannaz, J.P. Guillet, E. Pilon: Z. Phys. C56 (1992) 589
19. L.E. Gordon, J.K. Storrow: Z. Phys. C56 (1992) 307
20. M. Diemoz, F. Ferroni, E. Longo, G. Martinelli: Z. Phys. C39 (1988) 21
21. A. Rostovtsev, V. Soloshenko: H1 Note H1-08/93-309 (August 1993); see also S. Frixione, M.L. Mangano, P. Nason, G. Ridolfi: Phys. Lett. B319 (1993) 339

This article was processed using Springer-Verlag TEX Z.Physik C macro package 1.0 and the AMS fonts, developed by the American Mathematical Society.